Exploring Thermoelectric Properties Enhancement Through Creation of Defects and Doping

Zawwar Shabahat Ahmed[1*]
1-American International School,United Nations Rd, Dhaka 1212, Bangladesh
*Email:zawwarsa2026@gmail.com

Abstract
Thermoelectric conversion provides a direct means of transforming a temperature difference into electrical energy and is therefore relevant to the recovery of otherwise unused heat. Copper sulfide (CuS) is an attractive thermoelectric host because it combines high electrical transport capability with relatively low thermal conductivity and a defect-rich crystal chemistry. In this work, selenium was introduced into CuS at nominal concentrations of 0.05, 0.10, and 0.15 to regulate both carrier transport and phonon propagation. The resulting Se–CuS materials were examined with respect to their crystal structure, microstrain, crystallite size, electrical conductivity, Seebeck coefficient, thermal conductivity, power factor, and thermoelectric figure of merit. X-ray diffraction confirmed that the characteristic CuS framework was retained after Se incorporation, while the progressive displacement and broadening of the diffraction peaks indicated lattice perturbation. Williamson–Hall analysis showed that the estimated microstrain increased from 4.9×10^{-5} to 8.8×10^{-5}, whereas the corresponding crystallite size decreased from about 35.3 to 29.3 nm as the Se content increased. Among the investigated compositions, 0.10 Se–CuS delivered the most favorable combination of thermoelectric properties, giving a Seebeck coefficient of about 52 μV K^{-1}, an electrical conductivity of 830.6 S cm^{-1}, and a power factor of 224.6 μW m^{-1} K^{-2} at 300 K. The thermal conductivity was reduced from 2.80 W m^{-1} K^{-1} for pristine CuS to 1.85 W m^{-1} K^{-1} for the 0.10 composition at 300 K, leading to a calculated maximum ZT of approximately 0.143 at 500 K. Finite-element calculations in COMSOL Multiphysics were additionally used to visualize temperature, heat-flow, and electrical-potential distributions under thermoelectric operating conditions. The results indicate that controlled Se incorporation can introduce useful structural disorder while retaining sufficient electronic transport, thereby providing a route for balancing phononic and electronic contributions in CuS-based thermoelectric materials.

Keywords: CuS; Se-doped CuS; thermoelectric materials; waste-heat recovery

1. Introduction

A considerable portion of the energy supplied to industrial facilities, transportation systems, power-generation units, and other energy-intensive operations is ultimately rejected as heat. A large fraction of this rejected energy occurs at temperatures for which conventional heat-recovery approaches are either inefficient or difficult to implement [1]. Thermoelectric technology offers an alternative because a temperature gradient can be converted directly into an electrical response without mechanical motion. The absence of moving parts is advantageous for compact and distributed systems, where reliability, low maintenance, silent operation, and long service life are important. Consequently, development of thermoelectric materials that combine high electrical performance with low heat conduction remains an important research direction for waste-heat utilization and solid-state energy conversion as shown in Figure 1.[2]

The performance of a thermoelectric material is commonly expressed through the dimensionless figure of merit, ZT, which is written as:

$$ZT = \frac{S^2 \sigma T}{\kappa} \qquad \text{(Eq 1)}$$

Here, S denotes the Seebeck coefficient, σ is the electrical conductivity, T is the absolute temperature, and κ is the total thermal conductivity. The product $S^2\sigma$ corresponds to the electrical power factor, whereas κ describes the ability of the material to transport heat. An effective thermoelectric material must therefore generate a strong thermoelectric voltage, maintain efficient charge transport, and simultaneously restrict heat flow. These requirements are intrinsically coupled. For instance, increasing the concentration of charge carriers can enhance electrical conductivity but may

reduce the Seebeck coefficient. Likewise, intense carrier scattering can lower electrical conductivity even though analogous scattering processes may be beneficial for suppressing lattice heat transport. Thermoelectric optimization consequently requires simultaneous consideration of electronic and phononic transport rather than maximization of a single parameter [3].

Well-established thermoelectric compounds such as Bi2Te3, PbTe, and Sb2Te3 have demonstrated strong performance, but their broader deployment can be constrained by material cost, elemental availability, toxicity concerns for lead-containing systems, and long-term sustainability considerations. These limitations have encouraged investigation of less expensive and more readily available alternatives. Metal chalcogenides are particularly interesting because their electronic structures and defect populations can be modified through compositional substitution, vacancies, and other forms of structural engineering. Copper chalcogenides are among the promising candidates because they can exhibit high electrical conductivity together with intrinsically low lattice thermal conductivity and complex defect chemistry [4], [5].

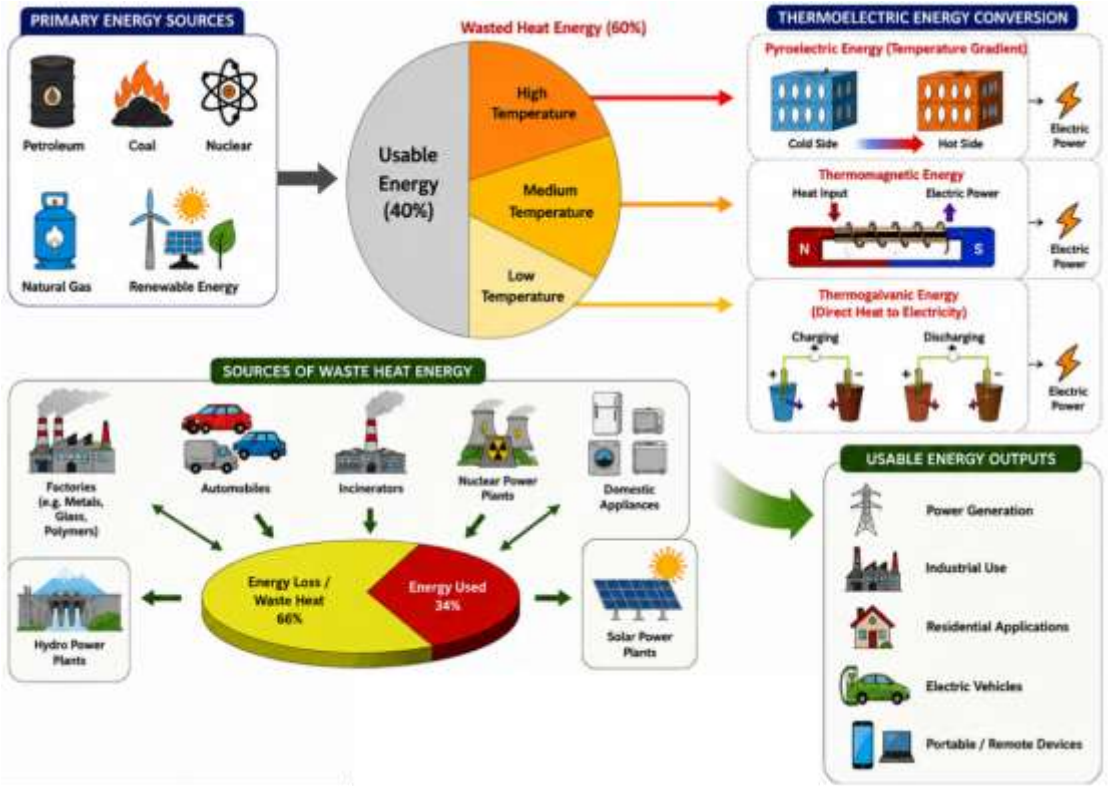


Figure 1. Schematic illustration of primary energy sources, major waste-heat sources, and the conversion of otherwise wasted thermal energy into useful electricity through thermoelectric and other solid-state energy-conversion technologies across different temperature ranges.

Copper sulfide is especially attractive for thermoelectric applications because both Cu and S are comparatively abundant and inexpensive. The Cu–S system contains several compositions and structural forms, including CuS and copper-deficient Cu2−xS phases. Its transport properties are strongly affected by copper vacancies, carrier density, phase composition, and the mobility of Cu ions. In copper-deficient chalcogenides, mobile Cu species and associated structural disorder can produce strong phonon scattering while preserving useful electronic transport. Consequently, copper sulfide and related compounds have been investigated as alternatives to conventional thermoelectric materials, with reported ZT values approaching the range of 1.5–2 for optimized copper-deficient sulfide and selenide compositions at elevated temperatures [6], [7].

Further improvement of CuS requires control over the balance between charge and heat transport. Elemental doping is one route for achieving such control because an introduced species can alter carrier concentration, carrier mobility, band structure, defect populations, and lattice dynamics. Depending on the dopant and its concentration, substitution may either improve or degrade the electrical response. The electrical conductivity is described by [8], [9]:

$$\sigma = ne\mu \quad \text{(Eq 2)}$$

where n is the concentration of mobile charge carriers, e is the elementary charge, and μ represents their mobility. A dopant can modify n through differences in valence and chemical environment, while changes in bonding and electronic states can affect μ and the Seebeck response. Excessive dopant incorporation, however, can introduce strong carrier scattering and thereby reduce mobility. An appropriate dopant concentration is therefore necessary to obtain a favorable power factor

The Seebeck coefficient is also closely connected to the electronic structure and carrier concentration. For a simplified single-carrier picture, increasing carrier concentration generally tends to lower the magnitude of S, which means that thermoelectric design involves a compromise between carrier density and charge mobility. Doping can help tune this balance by shifting the Fermi level and modifying the density of electronic states. Changes in local bonding and atomic configuration may further influence the effective mass and energy dependence of carrier transport[10].

Doping is also an important strategy for reducing thermal conductivity. The total thermal conductivity can be expressed as

$$\kappa = \kappa_e + \kappa_l \quad \text{(Eq 3)}$$

where κ_e and κ_l are the electronic and lattice contributions, respectively. In many thermoelectric materials, reducing the lattice contribution is particularly useful. When a foreign atom is incorporated into a host lattice, differences in atomic mass, size, bonding strength, and local force constants can generate mass disorder and strain fields. These perturbations interrupt phonon propagation and increase phonon scattering, shortening the phonon mean free path and lowering lattice thermal conductivity. Vacancies, interfaces, grain boundaries, and other structural imperfections can provide additional scattering pathways over different length scales [11], [12].

Defect engineering is therefore an important strategy for independently influencing charge and heat transport. Point defects are effective at scattering short-wavelength phonons, whereas nanoscale interfaces, precipitates, and grain boundaries can interact with longer-wavelength phonons. A distribution of defects across multiple length scales can consequently reduce lattice heat conduction while retaining useful electronic transport when the defect density is carefully controlled [13], [14].

In the present study, Se was selected as a substitutional dopant for CuS. Because Se belongs to the same chalcogen family as S, its incorporation provides a chemically compatible means of perturbing the Cu–S framework. The larger atomic radius and greater atomic mass of Se relative to S are expected to produce local lattice expansion, strain, mass fluctuations, and changes in Cu–chalcogen bonding. These effects can alter the crystal structure and electronic environment while also introducing additional phonon-scattering centers.

Se substitution may also modify the electronic response of CuS through differences in orbital energy, polarizability, and bonding characteristics. Such changes can affect the density of states and the population and mobility of charge carriers. Because copper vacancies are important to transport in copper chalcogenides, changes in their chemical environment following Se incorporation may provide an additional mechanism for regulating conductivity.

The effect of Se concentration is therefore expected to arise from competing electronic and phononic contributions. At an appropriate dopant level, lattice distortion and mass disorder can strengthen phonon scattering and lower thermal conductivity while the electronic structure remains favorable for charge transport. At higher loading, however, excessive disorder or secondary-phase formation may increase carrier scattering and reduce the electrical response. Determining the optimum Se concentration is consequently essential for obtaining a suitable compromise among S, σ, and κ [15].

Accordingly, Se-doped CuS with nominal Se concentrations of 0, 0.05, 0.10, and 0.15 was investigated as a compositionally engineered thermoelectric system. The study correlates structural changes and microstrain with temperature-dependent electrical conductivity, Seebeck coefficient, thermal conductivity, power factor, and ZT. Finite-element simulations were also used to examine temperature and electrical-potential distributions under thermoelectric operating conditions, providing a numerical complement to the experimental measurements [16].

2. Materials and Methods

2.1 Materials

Copper(II) acetate monohydrate ($Cu(CH_3COO)_2 \cdot H_2O$, ≥99%), sodium thiosulfate pentahydrate ($Na_2S_2O_3 \cdot 5H_2O$, ≥99%), selenium powder (Se, ≥99.5%), and other reagents of analytical grade were purchased from commercial suppliers and used without further purification. Deionized water was used throughout the synthesis.

2.2 Synthesis of Se-doped CuS (Se–CuS)

A series of $CuS_{1-x}Se_x$ compositions was prepared with x = 0, 0.05, 0.10, and 0.15 using a wet-chemical procedure. For each composition, the required quantities of copper acetate and selenium powder were dispersed in deionized water under continuous agitation. An aqueous sodium thiosulfate solution was subsequently introduced dropwise while stirring was maintained, providing the sulfur source. The reaction mixture was kept at 90 °C in an oil bath for 6 h. After the reaction was allowed to cool to room temperature, the solid product was recovered by centrifugation. The precipitate was repeatedly rinsed with deionized water followed by absolute ethanol and then dried under vacuum at 60 °C for 12 h. The resulting powder was compacted hydraulically into pellets approximately 8 mm in diameter for thermoelectric characterization.

Table 1. Stoichiometric amounts of copper, sulfur, and selenium precursors used for the synthesis of $CuS_{1-x}Se_x$ samples.

Sample	x	Cu acetate monohydrate	$Na_2S_2O_3.5H_2O$	Se powder
CuS	0	199.65 mg	248.18 mg	0 mg
$CuS_{0.95}Se_{0.05}$	0.05	199.65 mg	235.77 mg	3.95 mg
$CuS_{0.9}Se_{0.1}$	0.10	199.65 mg	223.36 mg	7.90 mg
$CuS_{0.85}Se_{0.15}$	0.15	199.65 mg	210.95 mg	11.84 mg

2.3 Characterization

The phase constitution and crystal structure of the prepared powders were evaluated by powder X-ray diffraction using Cu Kα radiation on a PANalytical instrument (Netherlands). The Seebeck coefficient and electrical conductivity were measured using a ULVAC-RIKO ZEM-3 thermoelectric measurement system under a partial He atmosphere.

2.4 COMSOL Multiphysics Simulation

Finite-element calculations were performed in COMSOL Multiphysics to examine the coupled thermal and electrical response of a CuS-based thermoelectric element subjected to a prescribed temperature difference. A three-dimensional representation of the thermoelectric pellet together with copper electrodes was constructed using the Heat Transfer in Solids and Electric Currents physics interfaces, which were coupled through the Thermoelectric Effect multiphysics formulation. Temperature-dependent Seebeck coefficient, electrical conductivity, and thermal conductivity values obtained from the thermoelectric analysis were assigned as material properties.

The two opposing faces of the thermoelectric element were assigned hot- and cold-side temperatures to establish the applied temperature gradient, while the remaining external surfaces were treated as thermally insulated. Electrical boundary conditions were imposed at the copper contacts so that the thermoelectric voltage generated across the Se–CuS element could be calculated. The coupled model simultaneously accounts for heat conduction and thermoelectric conversion and therefore permits evaluation of temperature and electrical-potential fields. Temperature, electric potential, heat flux, and current-density distributions were extracted from the simulations. The calculated potential difference between the electrodes was used to estimate the thermoelectric voltage generated under the imposed thermal gradient, while the heat-flux field was examined to understand heat transport through the active material. The simulated response was then compared conceptually with the measured transport properties and calculated power factor and ZT.

3. Results

The phase structure of pristine and Se-containing CuS was examined by powder X-ray diffraction (Figure 2a). The diffraction pattern of undoped CuS contains the characteristic reflections associated with the CuS framework, confirming formation of the crystalline sulfide phase. After introduction of 0.05, 0.10, and 0.15 Se, the principal CuS reflections remain visible, indicating that the host structure is retained over the investigated composition range. No distinct diffraction features attributable to crystalline elemental Se or a clearly resolved secondary Se-containing phase were detected within the sensitivity of the measurement.

With increasing Se concentration, the CuS reflections exhibit a small shift toward lower 2θ together with progressive broadening. The peak displacement is consistent with the larger atomic size of Se relative to S and can be associated with local lattice expansion. The broadening, in turn, can arise from changes in crystallite dimensions and increased microstrain generated by dopant incorporation.

Williamson–Hall analysis (Figure 2 b) was applied to separate the contributions of crystallite size and lattice strain to the observed broadening. The relation used was:

$$\beta\cos\theta = \frac{K\lambda}{D} + 4\varepsilon\sin\theta \qquad \text{(Eq 4)}$$

In this expression, β is the corrected full width at half maximum expressed in radians, θ is the Bragg angle, K is the shape factor (taken as approximately 0.9), λ is the wavelength of Cu Kα radiation, D is the volume-weighted crystallite size, and ε denotes the lattice microstrain. A plot of βcosθ against 4sinθ provides the microstrain from the slope and the crystallite size from the intercept.

The Williamson–Hall results show a systematic increase in slope as the Se concentration is raised. The calculated microstrain changes from approximately 4.9×10^{-5} for 0.05 Se to 6.7×10^{-5} and 8.8×10^{-5} for the 0.10 and 0.15 compositions, respectively. Over the same range, the estimated crystallite size decreases from about 35.3 nm to 32.2 and 29.3 nm. This trend indicates that Se incorporation progressively perturbs the CuS lattice and limits the development of larger, highly ordered crystallites.

The structural changes provide a plausible basis for the observed thermoelectric behavior. Higher microstrain, smaller crystallites, lattice imperfections, and grain boundaries introduce additional sites at which heat-carrying phonons can be scattered. Such disorder can reduce the lattice contribution to thermal conductivity, provided that the associated structural perturbations do not excessively impede electronic transport.

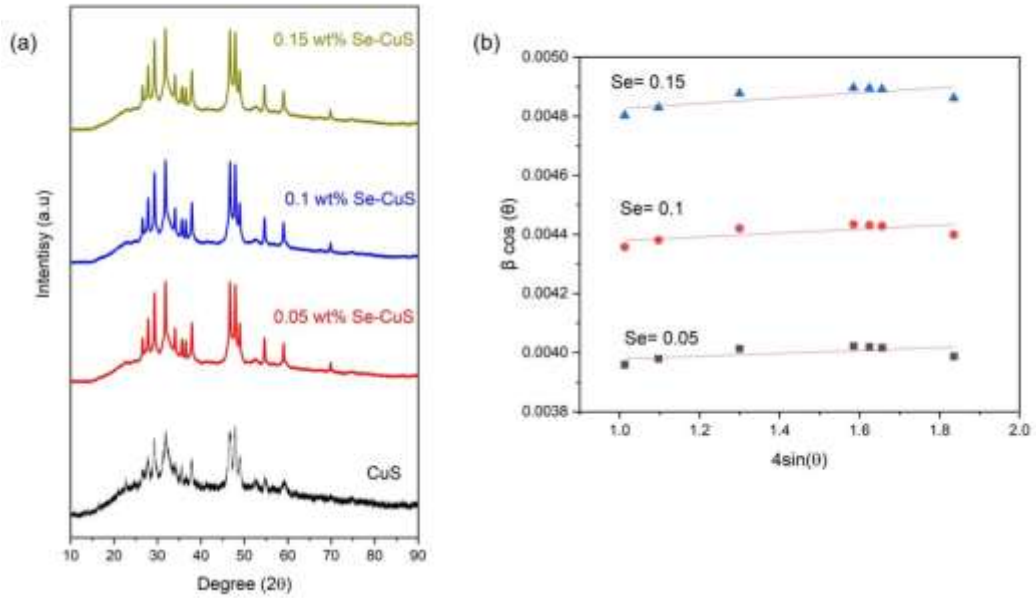


Figure 2. (a) Powder X-ray diffraction (XRD) patterns of pristine CuS and Se-doped CuS containing 0.05, 0.10, and 0.15 Se; (b)Williamson–Hall plots of the Se-doped CuS samples obtained from the relationship between βcosθ and 4sinθ.

The Seebeck coefficient, electrical conductivity, thermal conductivity, power factor, and ZT were determined between 300 and 500 K for pristine CuS and the three Se-doped compositions. The systematic variation with Se concentration demonstrates that relatively small amounts of Se can simultaneously alter electronic and thermal transport. The Seebeck coefficient (Figure 3a) rises with temperature for every composition. For pristine CuS, S increases from approximately 32 μV K^{-1} at 300 K to about 43 μV K^{-1} at 500 K. At 300 K, the 0.05, 0.10, and 0.15 Se samples exhibit Seebeck coefficients of approximately 41, 52, and 47 μV K^{-1}, respectively. The 0.10 Se–CuS composition maintains the strongest thermopower over the investigated temperature interval and reaches about 67 μV K^{-1} at 500 K. The increase in S following moderate Se incorporation is consistent with a dopant-induced modification of the electronic structure and carrier concentration. The lower value observed for the 0.15 composition suggests that further Se addition introduces transport disorder that offsets the beneficial effect.

Electrical conductivity (Figure 3b) follows a similar composition-dependent trend. At 300 K, pristine CuS exhibits a conductivity of approximately 399 S cm^{-1}, whereas the 0.05, 0.10, and 0.15 Se compositions give approximately 554, 831, and 711 S cm^{-1}, respectively. The 0.10 Se sample therefore provides the highest conductivity among the investigated materials and reaches about 915 S cm−1 at 500 K. The improvement at moderate Se loading may arise from changes in carrier concentration and the available transport pathways. When the Se concentration is increased to 0.15, the conductivity decreases relative to the 0.10 sample, suggesting that additional disorder begins to enhance carrier scattering.

The thermal conductivity (Figure 3c) shows the opposite composition dependence. At 300 K, the value decreases from about 2.80 W m^{-1} $K^{-1}$for pristine CuS to 2.35, 1.85, and 2.05 W m^{-1} K^{-1} for the 0.05, 0.10, and 0.15 Se materials, respectively. The thermal conductivity also decreases with increasing measurement temperature, reaching approximately 1.94 W m^{-1} K^{-1} for pristine CuS and 1.35 W m^{-1} K^{-1} for the 0.10 composition at 500 K. The reduction in heat transport can be associated with the structural disorder produced by Se substitution. The increased microstrain and reduced crystallite size identified from the Williamson–Hall analysis provide additional phonon-scattering centers and thereby impede lattice heat propagation.

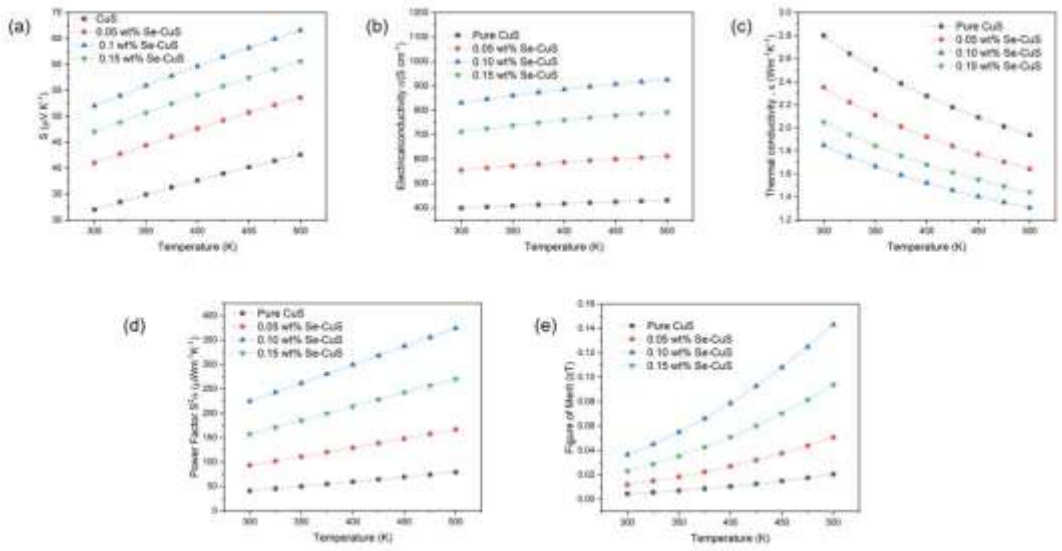


Figure 3. Temperature-dependent thermoelectric properties of pristine CuS and Se-doped CuS with different Se concentrations: (a) Seebeck coefficient (S), (b) electrical conductivity (σ), (c) thermal conductivity (κ), (d) power factor (S2σ), and (e) thermoelectric figure of merit (ZT) over the temperature range of 300–500 K.

The combined influence of thermopower and electrical conductivity is reflected in the power factor, PF = $S^2\sigma$ (Figure 3d) . For all compositions, PF increases with temperature, while the Se-containing samples consistently outperform pristine CuS. At 300 K, the power factor increases from approximately 40.9 μW m^{-1} K^{-2} for pristine CuS to 93.1, 224.6, and 157.0 μW m^{-1} K−2 for the 0.05, 0.10, and 0.15 Se samples, respectively. The 0.10 composition reaches approximately 374 μW m^{-1} K^{-2} at 500 K, indicating that this composition provides the most favorable compromise between Seebeck response and electrical transport.

The resulting ZT (Figure 3e) values increase with temperature for all compositions because the temperature dependence of the power factor and thermal conductivity acts together to improve the overall thermoelectric response.

At 500 K, the calculated ZT values are approximately 0.020, 0.051, 0.143, and 0.094 for pristine CuS, 0.05 Se–CuS, 0.10 Se–CuS, and 0.15 Se–CuS, respectively. The highest value, approximately 0.143, is obtained for the 0.10 Se material.

The enhanced response of the 0.10 composition can be understood as the result of two complementary effects: moderate Se incorporation strengthens phonon scattering and lowers thermal conductivity, while the electronic transport remains sufficiently favorable to maintain a high power factor. At 0.15 Se, the additional structural disorder appears to become detrimental to carrier transport, leading to lower S and σ and, consequently, a reduction in ZT. These observations indicate that an intermediate dopant level is preferable to maximum Se incorporation when the objective is to balance electronic and lattice transport.

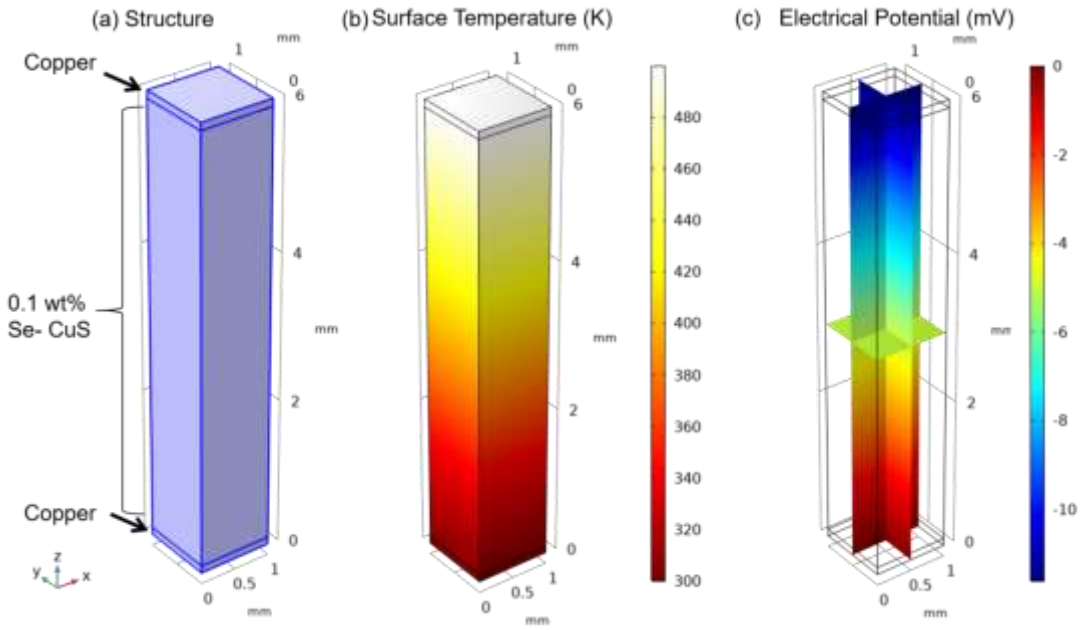


Figure 4. Finite-element simulation of the thermoelectric response of the 0.1 Se–CuS sample under an applied temperature gradient: (a) three-dimensional geometry of the Cu–Se–CuS–Cu thermoelectric structure, (b) simulated surface-temperature distribution, and (c) corresponding electrical-potential distribution across the Se–CuS thermoelectric leg.

To examine the coupled thermal and electrical response of the optimized 0.10 Se–CuS composition, a three-dimensional COMSOL Multiphysics model was constructed (Figure 4). The simulated element was placed between copper electrodes, representing the essential geometry used for thermoelectric measurements. The Se–CuS leg was modeled on a millimeter scale and electrically contacted at its opposing surfaces.

A temperature difference was applied between the two ends of the thermoelectric leg, producing a predominantly one-dimensional temperature gradient along its length. The calculated temperature field extends from approximately 300 K at the cold side to 500 K at the hot side. The continuous temperature variation across the element demonstrates the establishment of the prescribed thermal gradient and indicates heat transfer through the active material.

The imposed temperature gradient generates an electrical-potential difference through the Seebeck effect. The simulated potential varies progressively along the Se–CuS leg, with values spanning approximately −10 to 0 mV for the modeled structure. This potential distribution represents the conversion of thermal energy into electrical energy under the applied gradient. The calculated voltage depends on the Seebeck coefficient, electrical conductivity, and local temperature field used as inputs to the model.

The simulation indicates that the optimized composition can sustain the imposed thermal gradient while generating a measurable electrical potential. Thus, the numerical results provide spatial information that complements the experimentally measured transport parameters and help visualize the coupled thermal-to-electrical response of the material.

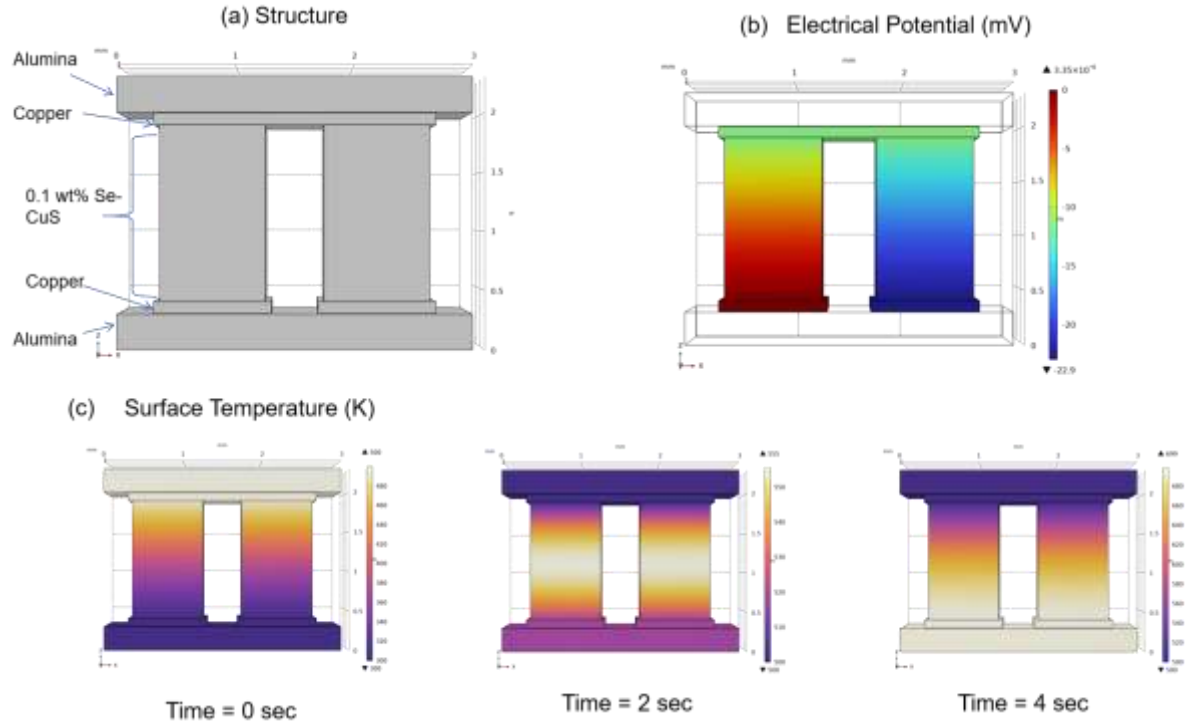


Figure 5. Three-dimensional COMSOL Multiphysics simulation of the Se–CuS thermoelectric cooler module: (a) model geometry showing the thermoelectric legs, Cu electrodes, and insulating/contact layers; (b) temperature distribution across the module under an applied electrical current; (c) simulated temperature distributions for different operating/boundary conditions, illustrating the development and variation of the hot and cold regions across the thermoelectric legs at 1 A.

The cooling behavior of the Se–CuS material was further examined through a three-dimensional COMSOL model representing a simplified Peltier module (Figure 5). The configuration contains two Se–CuS thermoelectric legs connected by electrically conducting copper electrodes. The Heat Transfer in Solids and Electric Currents interfaces were coupled to represent the interaction between heat flow and electrical transport.

When an electrical bias is applied, the calculated temperature field develops a difference between the two sides of the thermoelectric legs. One side becomes warmer while the opposite side is cooled, consistent with Peltier heat transport. The two Se–CuS legs display broadly similar temperature profiles, indicating that both contribute to the overall cooling response.

Additional simulated temperature distributions illustrate how the thermal field evolves under the selected operating conditions. The magnitude and spatial distribution of the temperature difference depend on the electrical transport properties of the Se–CuS material, applied current, thermal conductivity, and thermal boundary conditions. Maintaining a sufficiently large temperature difference is essential for effective thermoelectric cooling.

Overall, the finite-element results demonstrate electrothermal coupling in the Se–CuS module and provide a spatial representation of heat redistribution under electrical operation. Together with the measured thermoelectric properties, these simulations suggest that Se–CuS may be relevant not only to waste-heat-to-electricity conversion but also to solid-state cooling and thermal-management applications.

4. Limitations

Several limitations should be considered when interpreting the present results. First, the investigated Se concentration range is limited to 0.05–0.15, and the identification of 0.10 as the best-performing composition is therefore specific to the concentration window examined here. A broader composition series would be required to determine whether an even lower or higher Se content could provide further improvement.

Second, although the XRD and Williamson–Hall results support Se-induced lattice distortion and crystallite refinement, these techniques do not by themselves provide direct confirmation of the local chemical environment or exact substitutional position of Se within the CuS lattice. High-resolution TEM, STEM-EDS/EELS, XPS, or X-ray

absorption spectroscopy would provide complementary evidence for establishing the local structural and chemical configuration.

From the thermoelectric perspective, the measured improvement results from simultaneous changes in Seebeck coefficient, electrical conductivity, and thermal conductivity, making it difficult to isolate the contribution of individual carrier and phonon parameters. Temperature-dependent Hall measurements would provide direct information on carrier concentration and mobility, while separate determination of electronic and lattice thermal conductivity would strengthen the proposed transport interpretation.

The COMSOL calculations are also dependent on the prescribed material parameters and boundary conditions. Quantitative validation would therefore benefit from comparison of simulated voltage, temperature, and heat-flux distributions with measurements obtained under identical device conditions. Finally, long-term thermal stability, resistance to oxidation, and performance during repeated thermoelectric cycling were not comprehensively evaluated and should be addressed before assessing sustained waste-heat-recovery applications.

5. Conclusion

Selenium incorporation provides an effective means of modifying the structural and thermoelectric response of CuS while preserving the characteristic host crystal framework. XRD measurements indicate that the CuS phase remains dominant across the investigated Se concentrations, whereas peak displacement and broadening reveal progressive lattice perturbation. Williamson–Hall analysis shows that the microstrain increases from approximately 4.9×10^{-5} to 8.8×10^{-5} while the crystallite size decreases from about 35.3 to 29.3 nm with increasing Se content.

The structural disorder introduced by Se is accompanied by changes in both electronic and thermal transport. The 0.10 Se–CuS composition provides the most favorable overall response, with a Seebeck coefficient of approximately 52 μV K^{-1}, electrical conductivity of 830.6 S cm^{-1}, and power factor of 224.6 μW m^{-1} K^{-2} at 300 K. Its thermal conductivity is reduced to approximately 1.85 W m^{-1} K^{-1} at 300 K, and the calculated ZT reaches about 0.143 at 500 K.

Finite-element simulations further show that the optimized Se–CuS element can sustain a substantial temperature gradient while developing an electrical potential, and the modeled Peltier configuration exhibits a corresponding electrothermal response. The lower performance of the 0.15 composition indicates that excessive dopant-induced disorder can begin to impair charge transport. Overall, the results demonstrate that controlled, rather than maximum, Se incorporation is beneficial for balancing electronic and phononic transport in CuS and provides a useful basis for further development of CuS-based thermoelectric materials.

Reference

[1] H. Han *et al.*, “Advancements in thermoelectric materials: optimization strategies for enhancing energy conversion,” *J. Mater. Chem. A*, vol. 12, no. 36, pp. 24041–24083, Sep. 2024, doi: 10.1039/D4TA03666B.

[2] M. Mukherjee, A. Srivastava, and A. K. Singh, “Recent advances in designing thermoelectric materials,” *J. Mater. Chem. C*, vol. 10, no. 35, pp. 12524–12555, Sep. 2022, doi: 10.1039/D2TC02448A.

[3] Y. Li *et al.*, “Hierarchical MoS2/CuS photonic nanostructure accelerating photothermoelectric conversion of bacterial cellulose based phase change materials,” *J. Colloid Interface Sci.*, vol. 702, p. 138863, Jan. 2026, doi: 10.1016/J.JCIS.2025.138863.

[4] E. Isotta and A. Zevalkink, “Chemical compensation meets bond engineering in skutterudites,” *Joule*, vol. 10, no. 2, p. 102321, Feb. 2026, doi: 10.1016/j.joule.2026.102321.

[5] P. Rawat and S. Kala, “A concise review on the progression of copper sulfide as a potential thermoelectric material: Synthesis and thermoelectric properties,” *Nano Express*, vol. 6, no. 1, p. 012001, Jan. 2025, doi: 10.1088/2632-959X/ADA6E7.

[6] M. S. Abdurrhaman, M. Diantoro, R. A. Pahlevi, A. N. R. Masruhah, and C. I. Yogihati, “Synthesis and Characterization of CuS-GO Nanocomposite as Thermoelectric Material,” *AIP Conf. Proc.*, vol. 3197, no. 1, Feb. 2025, doi: 10.1063/5.0240589/3336453.

[7] K. V. Nabeela and P. P. Pradyumnan, “Reinforcement in thermoelectric properties of graphene nanoplatelets integrated covellite CuS nanocomposites for green heat harvesting applications,” *J. Alloys Compd.*, vol. 1050, p. 185480, Jan. 2026, doi: 10.1016/J.JALLCOM.2025.185480.

[8] S. I. Basha, S. S. Shah, and D. Y. Yoo, “Advancements in thermoelectric properties of cement and

geopolymer composites reinforced with carbon-based nanomaterials," *J. Build. Eng.*, vol. 104, p. 112312, Jun. 2025, doi: 10.1016/J.JOBE.2025.112312.

[9] Z. Li *et al.*, "Plasticity of Bi2Te3-family thermoelectric crystals," *Nat. Commun. 2025 161*, vol. 16, no. 1, pp. 5190-, Jun. 2025, doi: 10.1038/s41467-025-60465-2.

[10] E. S. Toberer, L. L. Baranowski, and C. Dames, "Advances in thermal conductivity," *Annu. Rev. Mater. Res.*, vol. 42, no. Volume 42, 2012, pp. 179–209, Aug. 2012, doi: 10.1146/ANNUREV-MATSCI-070511-155040/CITE/REFWORKS.

[11] K. F. Lunn and D. Apelian, "Thermal and Electrical Conductivity of Aluminum Alloys: Fundamentals, structure-property relationships, and pathways to enhance conductivity," *Mater. Sci. Eng. A*, vol. 924, p. 147766, Feb. 2025, doi: 10.1016/J.MSEA.2024.147766.

[12] Q. Mao, Y. Liu, and Y. Zhao, "A review on copper alloys with high strength and high electrical conductivity," *J. Alloys Compd.*, vol. 990, p. 174456, Jun. 2024, doi: 10.1016/J.JALLCOM.2024.174456.

[13] P. Muhammad *et al.*, "Defect Engineering in Nanocatalysts: From Design and Synthesis to Applications," *Adv. Funct. Mater.*, vol. 34, no. 29, p. 2314686, Jul. 2024, doi: 10.1002/ADFM.202314686.

[14] F. Liu and Z. Fan, "Defect engineering of two-dimensional materials for advanced energy conversion and storage," *Chem. Soc. Rev.*, vol. 52, no. 5, pp. 1723–1772, Mar. 2023, doi: 10.1039/D2CS00931E.

[15] Q. Xiong, G. Han, G. Wang, X. Lu, and X. Zhou, "The Doping Strategies for Modulation of Transport Properties in Thermoelectric Materials," *Adv. Funct. Mater.*, vol. 34, no. 52, p. 2411304, Dec. 2024, doi: 10.1002/ADFM.202411304;ISSUE:ISSUE:DOI.

[16] C. Wu *et al.*, "Defect EngineeringAdvances Thermoelectric Materials," *ACS Nano*, vol. 18, no. 46, pp. 31660–31712, Nov. 2024, doi: 10.1021/ACSNANO.4C11732.